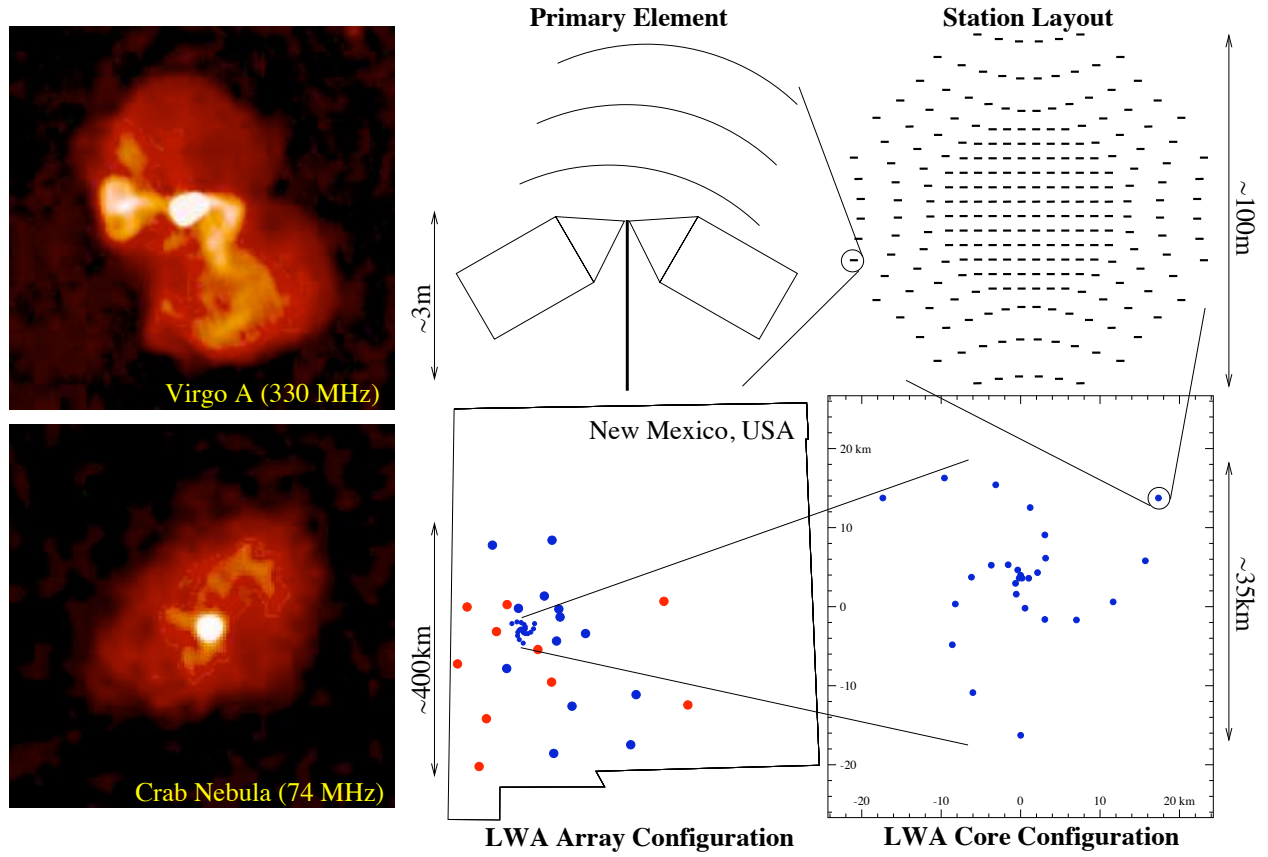


The Long Wavelength Array: Design Concept



Namir E. Kassim, T. Joseph W. Lazio, & William C. Erickson

CONTENTS

1. ASTROPHYSICALLY DRIVEN ARRAY PROPERTIES	1
1.1. Frequency Range	1
1.2. Angular Resolution and Array Size	1
2. TECHNICAL CONSIDERATIONS	2
2.1. Field of View	2
2.2. Sensitivity	2
2.3. Wide-Field Imaging	3
2.4. Radio Frequency Interference	5
2.5. Ionospheric Compensation	5
3. THE LWA CONCEPT	8
3.1. Frequency Range and Bandwidth	8
3.2. The Array Configuration	10
3.3. The Array Site	11
4. ACKNOWLEDGEMENTS	11

Chapter 1

Astrophysically Driven Array Properties

1.1 Frequency Range

Frequency versatile low-frequency observations are powerful diagnostics of emission, absorption, and scattering phenomena. For emission the instrument can provide superior point-source and surface-brightness sensitivity to steep-spectrum sources, accurately constraining emission spectra. This drives the observing frequencies to the limit allowed by the ionosphere. Even above the LW range ($\nu < 100\text{MHz}$) only a few existing instruments can make measurements (e.g., Cambridge and GMRT at 151 MHz, the VLA and Westerbork at 330 MHz) but only the VLA at 74 MHz provide imaging capabilities at lower frequencies. (The GMRT's angular resolution will be a few arc-minutes, well above that planned for the LWA.)

The case of absorption is perhaps more interesting. Here the interaction of nonthermal emitting sources with absorbing thermal material allows unique observations for probing the distribution of both the emitters and absorbers. The case of constraining cosmic-ray properties by measuring the foreground emission along lines of sight to absorbing H II regions has already been discussed. Furthermore, low-frequency observations are key to studying intrinsic self-absorption processes, such as synchrotron self-absorption in compact extragalactic sources. The key here is that all of these absorption effects are best studied at frequencies below 100 MHz where the observable properties of the radio universe acquire a completely different character because of absorption effects.

These scientific considerations direct us to as low a frequency as possible above the ionospheric absorption cutoff near 10 MHz. However, past experience has also taught us that ionospheric scintillations, which cannot be removed by self-calibration, will degrade a non-negligible fraction of the data below roughly 30 MHz. Thus, we plan for an instrument which can reach 20 MHz, with a realization that it will operate with reduced efficiency below 30 MHz. We are also limited at the high end by the radio FM bands at and above 87 MHz. Therefore, we plan for a broad band antenna, operating in the range of 20-80 MHz.

1.2 Angular Resolution and Array Size

Poor angular resolution is the single greatest limitation that has reduced the scientific yield of previous low-frequency instruments. In general, observations below 100 MHz have been limited to

angular resolutions of tens of minutes of arc or more. This is not sufficient to resolve most of the interesting structures. Hence sub-arcminute resolution would open up a completely new window on this region of the electromagnetic spectrum. Experience from low-frequency VLBI measurements shows that very few sources exhibit compact structure which can be detected with reasonable sensitivities on baselines longer than 400 km. Thus, a reasonable goal would be an array whose longest dimensions were approximately 400 km, rendering approximately 8" and 2" resolution at 20 and 80 MHz, respectively. This nicely places the maximum resolution at the lower frequencies just above the natural limit set by interstellar and interplanetary scattering Weiler et al. 1990.

Chapter 2

Technical Considerations

The new NRL-NRAO 74 MHz observing system at the VLA is the first to break the “ionospheric barrier” successfully and demonstrates that interferometry at low frequencies can now be extended to baselines far longer than the 3-km scale previously thought to be dictated by the ionosphere. In §3, we capitalize on this breakthrough and present our proposal for the LWA, a much larger and broad-band instrument that could tackle the many interesting scientific problems outlined above. Here we discuss critical calibration and imaging issues unique to this type of instrument, and we extend the results developed by Perley & Erickson (1984) in their initial consideration of a 74 MHz system for the VLA. Extensive simulations are required to confirm these approximations and drive the detailed design of any much larger system.

2.1 Field of View

The phase fluctuations introduced by the ionosphere can be tracked by self-calibration as time-variable contributions to the antenna-based phase solutions. However if the field of view is larger than the “isoplanatic patch,” then the time variable ionospheric phases take on a positional dependence as well. New imaging algorithms (e.g., field-based calibration) address this problem and have been used successfully for the 74 MHz VLA. Even more sophisticated algorithms will be required for the LWA if it is to reach its angular resolution goals. However, this problem would be somewhat mitigated if the field of view can be reduced. This will ideally be done by grouping together individual dipole antennas into “stations” consisting of about 200 dipoles linked in a phased array and functioning like a single VLA antenna. The physical size of the station would determine the size of the beam. The LWA would then consist of an array of about 50 such stations spread throughout the state of New Mexico to provide baselines up to 400 km.

2.2 Sensitivity

Sensitivity issues at long wavelengths are unique. Two important characteristics are that the system temperature (i.e., thermal noise) is dominated by the sky brightness, and that confusion from

Fig. 1—Flux Density Available for Calibration at 74 MHz

f	S_{mod} (Jy)	S_{min} (Jy)	N
1.0	9.8	0.0036	167
0.75	7.3	0.12	10.2
0.50	4.9	0.91	2.0
0.25	2.5	4.0	0.25
0.10	1.0	14.2	0.04

background sources is significant. Perley & Erickson (1984) explored these issues for the 74 MHz VLA, and here we present results of that study modified for the much larger LWA proposed in §3. The thermal noise contributed by the Galactic background scales as $\nu^{-0.55}$. For directions away from the plane, the equivalent system thermal noise on an individual baseline, S_{thermal} is

$$S_{\text{thermal}} = 50 \text{ Jy} \left(\frac{408}{\nu} \right)^{2.55} \left(A_{\text{eff}} \sqrt{t \Delta \nu} \right)^{-1}. \quad (1)$$

Here ν is the observing frequency in MHz, A_{eff} is the collecting area of an individual station in m^2 , $\Delta \nu$ is the receiver bandwidth in MHz, and t is the integration time in seconds. The confusion noise arises from the contribution to the system temperature from unmodeled sources in the field of view (main beam confusion) and background sources rumbling through the sidelobes (sidelobe confusion). Extending the results of the random-walk analysis presented by Perley & Erickson (1984) to the case of a 200 km baseline, the equivalent system confusion noise is given by

$$S_{\text{confusion}} = 6.6 \text{ Jy} \left(\frac{408}{\nu} \right)^{0.75} (\nu t \Delta \nu)^{-1/2}. \quad (2)$$

This expression assumes that 50% of the flux in the main field of view can be reasonably modeled. Table 1 shows that this is always a good assumption. The first column is f , the fraction of the total flux in a 1° field of view at 74 MHz that is available for modeling. The second column S_{mod} shows the total flux in the model, indicating that a typical 1° field will contain 9.8 Jy of flux. The third column, S_{min} , lists the weakest source in the model, while the last column, N , lists the total number of sources. The case of 50% modeling corresponds to $f = 0.5$, and Table 1 shows that 50% of the total flux in the field will be contained in only two sources. This means that simple starting models for self-calibration (e.g., two point sources) should work well.

Equations (1) and (2) can now be compared to show that for the LWA stations ($A_{\text{eff}} \sim 10^3 \text{ m}^2$ at 74 MHz), the confusion and thermal-noise contributions are comparable. From this approximation we calculate that the LWA described in §3 can achieve millijansky-level sensitivity in reasonable integration times, e.g., 0.5–1 mJy at 74 MHz for an 8-hour integration and 3-MHz bandwidth. Additional calculations presented in §3 (see Table 6) were made under this assumption.

2.3 Wide-Field Imaging

A conventional two-dimensional inversion of the three-dimensional visibility function measured by non-coplanar (i.e., non-east-west) arrays introduces phase errors which can become severe at

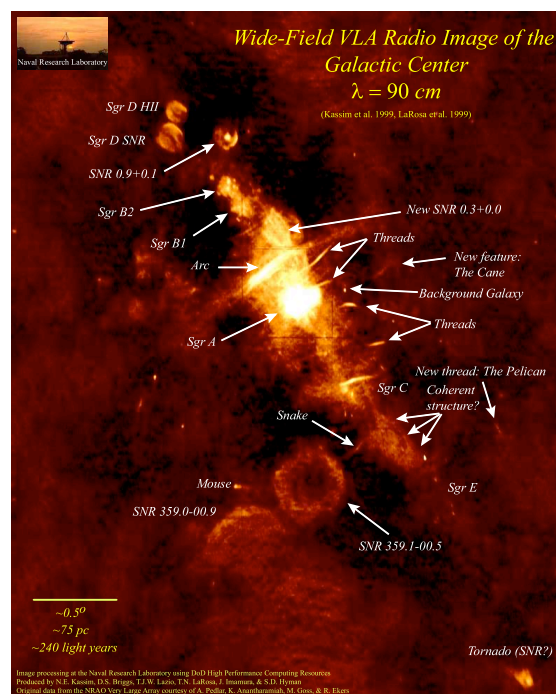


Fig. 2—A 330 MHz image of the Galactic center obtained with the VLA. This image covers $4^\circ \times 4^\circ$ at a resolution of $48'' \times 48''$. The rms noise level (excluding the bright sources on the Galactic ridge) is $5.9 \text{ mJy beam}^{-1}$.

long wavelengths (Perley 1989). The phase error goes as $w\theta^2$, where w is the third dimension in the visibility plane, perpendicular to the standard u - v plane, and θ is the distance from the phase center. The “3-D problem” arises when the entire primary beam (i.e., θ large), which may contain hundreds of discrete sources at the wavelengths under consideration, must be properly deconvolved. Numerical solutions to this problem have now been successfully implemented within a used astronomical data reduction packages (AIPS), with the only limitation being the high computational expense. For example AIPS can now implement a polyhedron algorithm in which the 3-D “image volume” is split into many 2-D “facets,” and is currently used to generate thermal-noise-limited images from 330 MHz VLA observations on a routine basis. Examples of successful wide-field, non-coplanar image deconvolutions are shown in Figure 2 for the Galactic center at 330 MHz (from SDE) and Figure 3 for the Coma cluster field at 74 MHz (from AIPS).

The computational driver for extending the polyhedron algorithm to lower frequencies is the number of facets N_{facet} that are required to divide up the surface of the image sphere, and $N_{\text{facet}} \propto \lambda B/D^2$, where B is the baseline length, λ is the observing wavelength, and D is the aperture size of the individual antenna elements (Perley 1989). For the 74 MHz VLA $N_{\text{facet}} \sim 225$, so that for an instrument with $B > 100$ km, thousands of facets may be required. Current scaled-processing platforms have already demonstrated the capability of reducing data with hundreds of facets, and in light of the continuing rapid advance in available computational power, practical solutions to the wide-field imaging problem should be readily available for the LWA.

2.4 Radio Frequency Interference

The long wavelength spectrum contains copious amounts of radio frequency interference (RFI) from terrestrial transmitters. These interfering signals are, however, at low enough levels that they do not overload the highly linear electronics modules that are available on today’s market at low prices. Experience has shown that sufficiently clear bands exist between the interfering signals to allow sensitive observations. In fact, the 74 MHz band at the VLA is one of the cleanest bands available to that instrument, and the radio band below 100 MHz is one of the few portions of the spectrum where RFI levels actually seem to be decreasing as many communication services move to higher frequencies or to optical fibers. Nevertheless, it will almost certainly be necessary to incorporate some RFI avoidance and excision procedures into the LWA system, but, with modern digital technology, this can be done relatively easily even for a correlator with many thousands of channels.

Though RFI excision algorithms will be needed, the problem can first be reduced with hardware in several ways. First, a site with relatively low levels of RFI should be chosen for the LWA. Second, dipoles should be designed to have very low sensitivity toward the horizons. Third, amplifiers should be designed to produce low levels of intermodulation. The bandpass of our front end filter is selected to minimize contributions from strong FM radio signals (88-108 MHz) within and outside (anti-aliasing) the Nyquist zone of interest. A high sampling rate has been chosen to dilute strong interference combined with a large number of bits for high dynamic range. Each beam can be independently pointed and tuned to an RFI-free band.

2.5 Ionospheric Compensation

The 74 and 330 MHz VLA systems demonstrate that self-calibration will successfully remove ionospheric phase effects when the full array signal-to-noise ratio is 3–5. Since the signal-to-noise ratio on an individual baseline is a factor of $N^{-1/2}$ times smaller than that available for an array of N individual stations an array of roughly 50 stations proposed in §3 would mean that we can

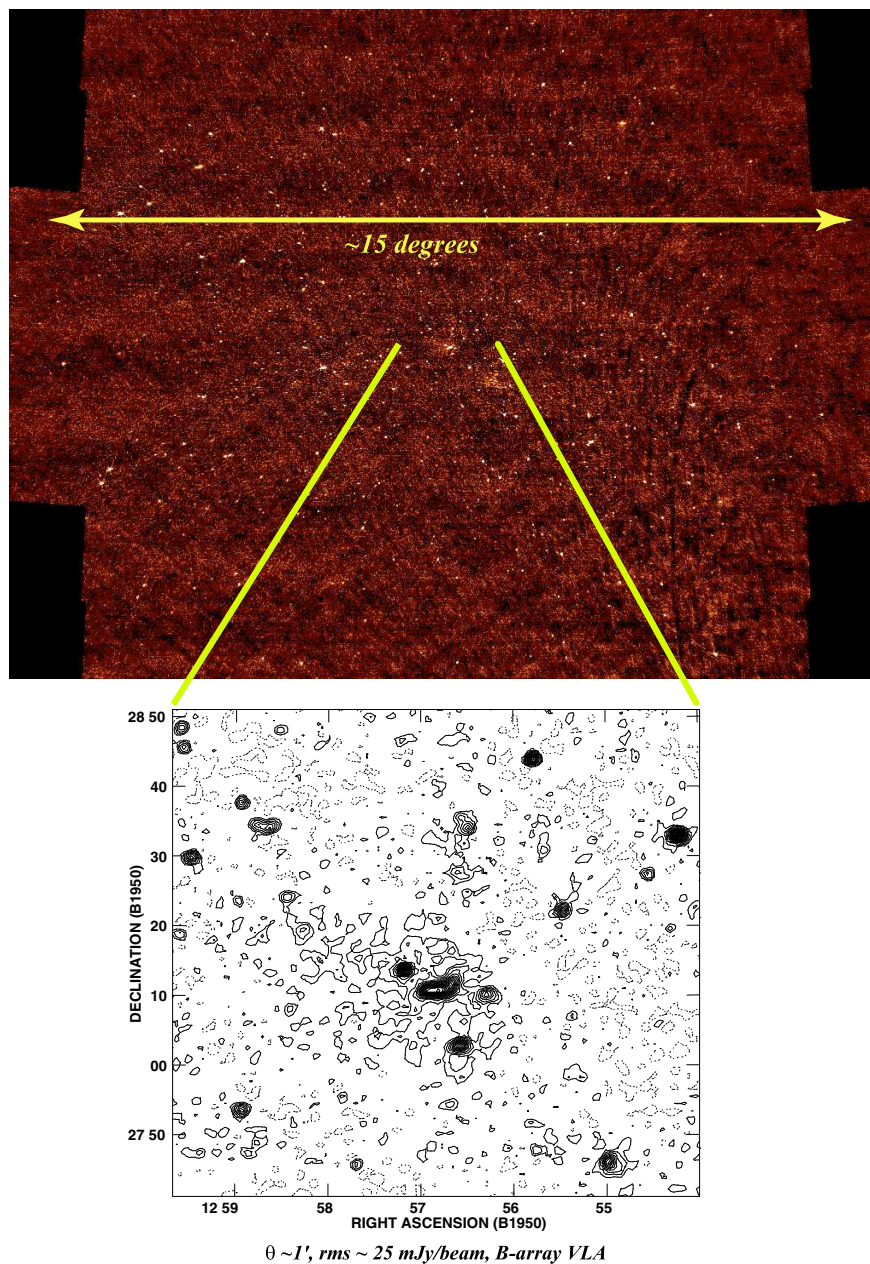


Fig. 3—The Coma cluster of galaxies at 74 MHz. (*Top*) The entire primary beam. This image illustrates the efficiency with which large sections of the sky can be mapped with a sensitive, low-frequency instrument. The rms noise level is 25 mJy beam^{-1} , and the field covers approximately 15° at a resolution of $1'$. (*Bottom*) A subimage of the wide-field image showing the central galaxies and the cluster halo.

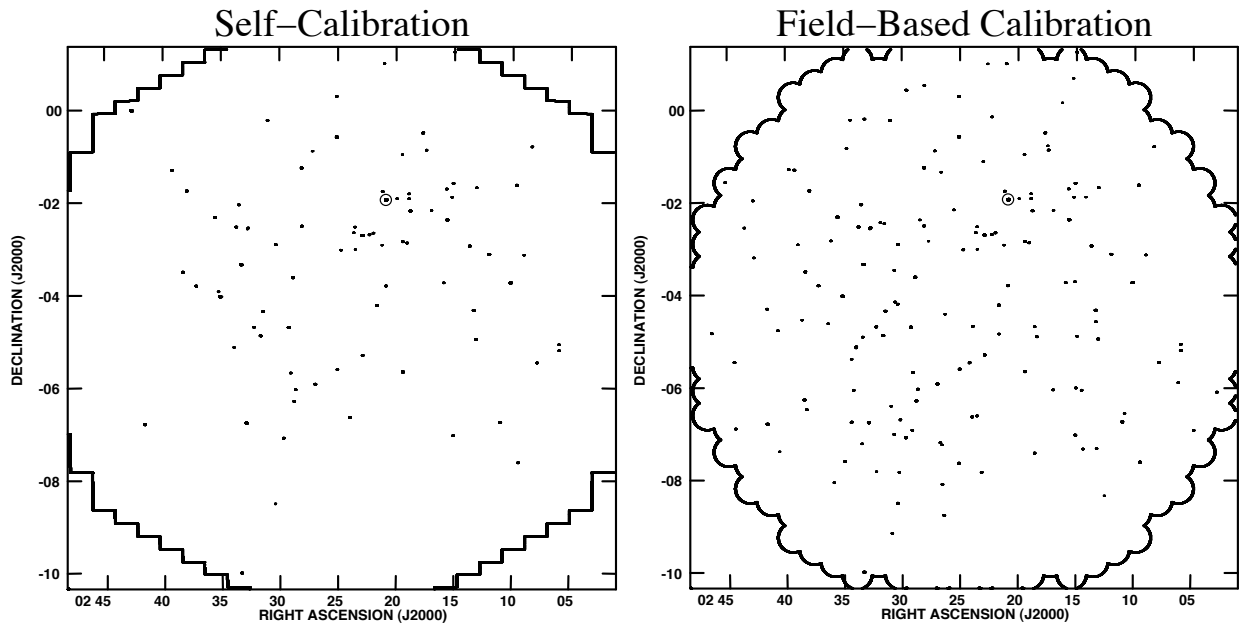


Fig. 4—Images of the 74 MHz primary beam area produced using self-calibration (left) and VLAFM (right). The bright source 3C 63 is circled. This is a contour map in which the first contour is set so far above the noise, $400 \text{ mJy } \text{bm}^{-1}$, that only actual sources appear. Since the synthesized beam is so small compared to the entire field, the sources simply appear as dots at this scale. Images from Cohen et al. 2003.

tolerate a signal-to-noise ratio on a single baseline of approximately 1 and still have convergence. Perley & Erickson (1984) have calculated the signal-to-noise ratio available for self-calibration under the assumption that the noise is thermal noise from the Galactic background and that the field of view of the instrument will be comparable with or less than the isoplanatic patch size. For 50% modeling and 1° field of view, they find that a baseline-based signal-to-noise ratio of unity can be achieved by bank collecting areas of $A_{\text{eff}} \sim 10^2 \text{ m}^2$. Since the values of A_{eff} proposed in §3 (see also Table 6) are greater than this, a self-calibration-based approach to ionospheric compensation will work successfully for the proposed array. Experience with the present 74 MHz VLA system already confirms this expectation.

The limitations of traditional self-calibration for imaging a full field of view can be seen in figure 4a. This image was produced with self-calibration. In this field a single bright source (3C 63, circled) has dominated the calibration, and one can expect the phase calibration to be accurate for this location. However because of ionospheric phase variations far from 3C 63, the refractive effects are different and sources will appear to wander as a function of time relative to the calibration center at 3C 63. This will cause the sources to be smeared in the time averaged image thereby lowering their apparent peak flux density. This is why the source density drops so dramatically with distance from 3C 63.

For full field imaging, rather than self-calibration a field-based calibration method, in which the phase calibration is position-dependent, is needed. Such an algorithm has been written by W.

D. Cotton and J. J. Condon¹ Cotton & Condon(2002). This algorithm models the ionosphere as phase screen varying in space and time, and applies a two-dimensional Zernike polynomial phase correction to correct the phases across the entire field of view. Our experience in applying this technique to 74 MHz VLA data has been extremely successful. A demonstration of this can be seen in figure 4b. Unlike in the self-calibrated image, of the same field, the source density in the field-based-calibrated image is uniform across the field of view.

Chapter 3

The LWA Concept

In this section we present our current strawman design for the LWA that can be used to estimate the various parameters involved in the construction of such a system. However, before any such instrument could be built, a detailed design study will be required. This design study may well result in significant changes to the proposal.

We envision crossed, linearly polarized dipoles as the individual receiving elements. The elements will be stationary and pointed vertically. These elements will be grouped into about 50 stations each containing about 250 dipoles within a roughly 100 meter diameter comprising a phased array. Each station beam can be steered to any point in the sky by tracking the phase delays of the individual elements within it. Beam steering would be entirely electronic (and thus instantaneous), and no mechanical devices would be used. Each station therefore functions like an individual antenna, and all the stations together form an interferometric array. Figure 5 shows a possible LWA layout.

3.1 Frequency Range and Bandwidth

The high-frequency limit of the instrument is driven both by the scientific work that can be accomplished with the high-angular-resolution images that can be formed at the higher frequencies and by the necessity of self-calibrating the images at the high-frequency end of the range. The phase information obtained from self-calibration is required for calibration of all lower-frequency images using DFIPR (Kassim et al. 1993; see also §2.5). However, the effective collecting area of the system is proportional to ν^{-2} , and at too high a frequency the antennas do not collect sufficient signal power for self-calibration. Also, there are strong RFI signals in the 87-108 MHz band which make this region of the spectrum unusable. Therefore, we plan to adopt a high-frequency limit of about 80 MHz.

The low-frequency limit determines the physical size of the individual antenna elements. Assuming that dipoles are used in the log-periodic elements, the dipoles must be approximately

¹VLA FM: a special-purpose task designed to work within AIPS

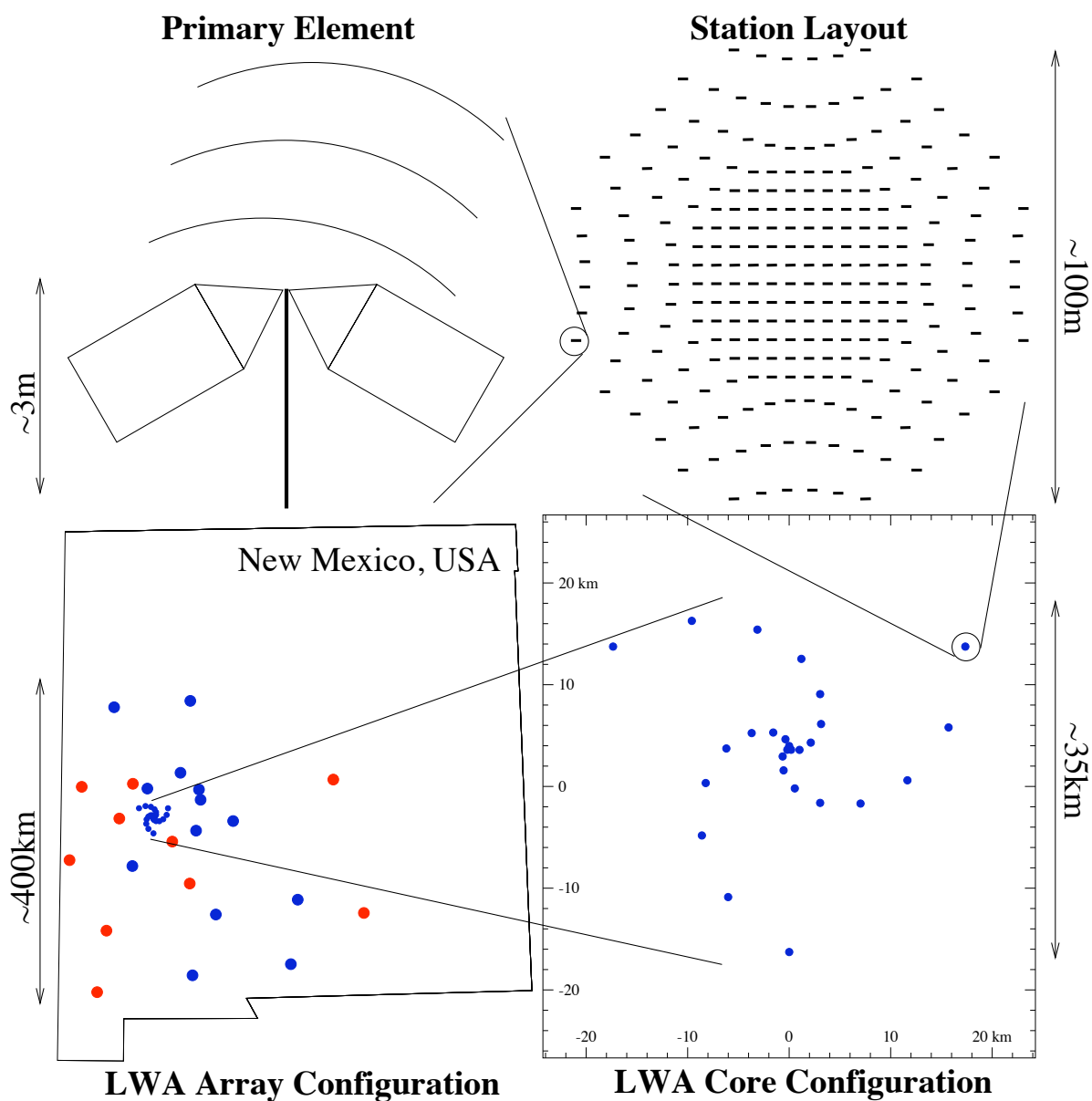


Fig. 5—A possible Long Wavelength Array layout. For the array configuration, planned NMA stations are shown in red. The compact core will likely be located a few kilometers to the west of the VLA.

Fig. 6—LWA specifications

Frequency range, bandwidth		20–80 MHz, 0.05–3.0 MHz
Total collecting area	@ 20 MHz	10^6 m ²
	@ 60 MHz	10^5 m ²
Angular resolution	@ 20 MHz	8''
	@ 80 MHz	2''
Pointing/frequency conversion time		< 1 ms
Sky coverage		< 60° zenith distance
Sensitivity ($\Delta\nu = 3$ MHz, $t = 8$ hr)	@ 20 MHz	~ 3 mJy
	@ 80 MHz	~ 1 mJy
Polarization		Full
Field of view	@ 20 MHz	$\sim 12^\circ$
	@ 80 MHz	$\sim 3^\circ$
Number of instantaneous baselines		1300
Time resolution		10 ms

one-half wavelength long at the low-frequency limit. A major portion of the cost of the system is in the antenna elements; larger elements are much more costly. Also, the antenna elements must be separated by more than a half wavelength at the low-frequency limit and this rather large separation leads to troublesome grating responses at the higher frequencies.

For broadband resonant antennas (eg. LPDA, zig-zag, or log-spiral) the wavelength of the low frequency limit is twice the maximum horizontal dimension. For the FAT2, the relation is not as simple, but for maximum collecting area at the low frequency limit, the minimum spacing is half the wavelength. At higher frequencies, such a spacing leads to troublesome grating responses. Another consideration at low frequencies is ionospheric amplitude scintillations. The phase variations scale precisely as λ provided that no amplitude scintillations are present, and this precise scaling is used for calibration of the low-frequency data (via DFIPR). However, at low frequencies there is enough angular refraction in ionospheric irregularities that rays passing through different irregularities can cross, causing constructive and destructive interference. This causes the apparent amplitude of the signal to scintillate and its phase to wander in an almost random fashion, making phase calibration virtually impossible. At most mid-latitude sites amplitude scintillation will occur about 30% of the time at frequencies below 30 MHz, making such observations impractical for this fraction of the time. Thus, some operation with diminished efficiency down to 20 MHz should be possible under particularly quiet ionospheric conditions.

Thus, we propose an instrument that is designed to operate in the frequency range 20 to 80 MHz, but with somewhat less efficiency in the range 20-30 MHz. Table 6 lists approximate LWA specifications.

3.2 The Array Configuration

The array configuration (ie. the location of each of the stations) is still in progress. The determining factors are: 1) the locations of the 10 NMA EVLA-2 antennas, 2) the existing optical-fiber networks and interconnections, 3) the existing road networks, and 4) the optical-fiber network

and other infrastructure of the VLA.

We will probably put stations at or near all of the 10 NMA antenna sites. The center of the LWA, which will consist of a more compact grouping of stations will not be at the VLA center, but close enough for us to take advantage of some of the VLA infrastructure. The remaining stations will be spread throughout the state of New Mexico in such a way as to produce the most uniform UV-coverage from the shortest baselines of about 400 m to the longest at up to 400 km, within the physical constraints listed above.

3.3 The Array Site

We consider the vicinity of NRAO's VLA near Socorro, New Mexico to be an advantageous location for the LWA. It has low external RFI levels and (with appropriate arrangements with NRAO) could make use of much pre-existing infrastructure such as fiber-optic links and roads. Also, the sites of the planned New Mexico Array (NMA) which is being proposed for the EVLA stage 2 will be at the correct distance from the VLA center to fulfill our need for baselines up to 400 km.

If the Frequency Agile Solar Radio telescope (FASR) is located in New Mexico, also near the VLA, colocating the core of the LWA and FASR might be practical and even synergistic for sharing infrastructure and support facilities.

Chapter 4

Acknowledgements

We thank D. Backer, T. Bastian, K. Blundell, P. Crane, J. Cordes, N. Duric, T. Enßlin, W. Farrell, P. Ray, L. J. Rickard, and A. Vourlidis for helpful comments.

The National Radio Astronomy Observatory is a facility of the National Science Foundation operated under cooperative agreement by Associated Universities, Inc. Basic research in radio

astronomy at the Naval Research Laboratory is supported by the Office of Naval Research.

Chapter 5

References

Cohen, A. S., Röttgering, H. J. A., Kassim, N. E., Cotton, W. D., Perley, R. A., Wilman, R., Best. P., Pierre, M., Birkinshaw, M., Bremer, M., & Zanichelli, A. 2003, “The Low-Frequency Radio Counterpart of the XMM Large-Scale Structure Survey” *ApJ* 591, 640

Cotton, W. D. & Condon, J. J. 2002, URSI General Assembly, 17-24 August, 2002, Maastricht, The Netherlands, paper 0944, pp 1-4.

Erickson, W. C., Mahoney, M. J., & Erb, K. 1982, “The Clark Lake Teepee-Tee telescope,” *ApJs*, 50, p. 403–419

Kassim, N. E., Perley, R. A., Erickson, W. C., & Dwarakanath, K. S. 1993, “Subarcminute Resolution Imaging of Radio Sources at 74 MHz with the Very Large Array,” *AJ*, 106, 2218–2228

Perley, R. A. 1989, “Imaging with non-coplanar arrays,” in *Synthesis Imaging in Radio Astronomy*, eds. R. A. Perley, F. R. Schwab, & A. H. Bridle (San Francisco: ASP) p. 259–275

Weiler, K. W. 1990. “Low frequency astrophysics with a space array,” in *Low Frequency Astrophysics from Space*, eds. N. E. Kassim & K. W. Weiler (Heidelberg: Springer-Verlag) p. 8–18